Airborne Observations Constrain Heterogeneous Nitrogen and Halogen Chemistry on Tropospheric and Stratospheric Biomass Burning Aerosol

Zachary C.J. Decker[1,2,3,a], Gordon A. Novak[1,2], Kenneth Aikin[1,2], Patrick R. Veres[1,b], J. Andrew Neuman[1,2], Ilann Bourgeois[1,2,c], T. Paul Bui[4], Pedro Campuzano-Jost[2,3], Matthew M. Coggon[1,2], Douglas A. Day[2,3], Joshua P. DiGangi[5], Glenn S. Diskin[5], Maximilian Dollner[6], Alessandro Franchin[1,2,7], Carley D. Fredrickson[8], Karl D. Froyd[1,2], Georgios I. Gkatzelis[1,2,d], Hongyu Guo[2,3], Samuel R. Hall[7], Hannah Halliday[5], Katherine Hayden[9], Christopher D. Holmes[9], Jose L. Jimenez[2,3], Agnieszka Kupc[1,2,6], Jakob Lindaas[11], Ann M. Middlebrook[1], Richard H. Moore[5], Benjamin A. Nault[12], John B. Nowak[5], Demetrios Pagonis[2,3,e], Brett B. Palm[8,b], Jeff Peischl[1,2], Felix M. Piel[13,14], Pamela S. Rickly[1,2,f], Michael A. Robinson[1,2,3], Andrew W. Rollins[1], Thomas B. Ryerson[1], Gregory P. Schill[1], Kanako Sekimoto[15], Chelsea R. Thompson[1], Kenneth L. Thornhill[5,16], Joel A. Thornton[8], Kirk Ullmann[7], Carsten Warneke[1], Rebecca A. Washenfelder[1,g], Bernadett Weinzierl[6], Elizabeth B. Wiggins[5], Christina J. Williamson[1,2,h,i], Edward L. Winstead[5,16], Armin Wisthaler[13,14], Caroline C. Womack[1,2], Steven S. Brown[1,3]

[1]NOAA Chemical Sciences Laboratory (CSL), Boulder, CO, USA

[2]Cooperative Institute for Research in Environmental Sciences, University of Colorado Boulder, Boulder, CO, USA

[3]Department of Chemistry, University of Colorado Boulder, Boulder, CO, USA

[4]NASA Ames Research Center, Moffett Field, CA, USA

[5]NASA Langley Research Center, MS 483, Hampton, VA, USA

[6]Faculty of Physics, Aerosol Physics and Environmental Physics, University of Vienna, Vienna, Austria

[7]Atmospheric Chemistry Observations and Modeling Laboratory, National Center for Atmospheric Research, Boulder, CO, USA

[8]Department of Atmospheric Sciences, University of Washington, Seattle, WA, United States

[9]Air Quality Research Division (AQRD), Environment and Climate Change Canada, Toronto M3H 5T4, Ontario, Canada

[10]Department of Earth, Ocean, and Atmospheric Science, Florida State University, Tallahassee, FL, USA

[11]Department of Atmospheric Science, Colorado State University, Fort Collins, CO, USA

[12]Center for Aerosol and Cloud Chemistry, Aerodyne Research, Inc., Billerica, MA, USA

[13]Institute for Ion Physics and Applied Physics, University of Innsbruck, 6020 Innsbruck, Austria

[14]Department of Chemistry, University of Oslo, 0315 Oslo, Norway

[15]Graduate School of Nanobioscience, Yokohama City University, Yokohama, Kanagawa, 236-0027, Japan

[16]Science Systems and Applications, Inc. (SSAI), Hampton, VA, USA

[a]Now at Laboratory of Atmospheric Chemistry, Paul Scherrer Institute (PSI), 5232 Villigen, Switzerland

[b]now at National Center for Atmospheric Research, Boulder, CO, USA

[c]now at Université Savoie Mont Blanc, INRAE, CARRTEL, 74200 Thonon-les-Bains, France

[d]Now at Institute of Energy and Climate Research, IEK-8: Troposphere, Forschungszentrum Jülich GmbH, Jülich, Germany

[e]now at Department of Chemistry and Biochemistry, Weber State University, Ogden, UT, USA

[f]now at Colorado Department of Public Health and Environment, 4300 Cherry Creek S Dr, Denver, CO, USA

[g]now at Cooperative Institute for Research in Environmental Sciences, University of Colorado Boulder, CO, USA

[h]now at Finnish Meteorological Institute, Erik Palmenin Aukio 1, 00560 Helsinki, Finland

[i]now at Institute for Atmospheric and Earth System Research/Physics, Faculty of Science, University of Helsinki, P.O. Box 64, 00014 Helsinki, Finland

Corresponding authors: Steven Brown (steven.s.brown@noaa.gov) and Zachary Decker (ZacharyCJDecker@gmail.com)

Key Points:

- N_2O_5 uptake coefficients are low on young biomass burning smoke and increase with transport through a PyroCB and UTLS aging
- $ClNO_2$ formation is active on biomass burning particles, but decreases with transport to the UTLS
- N_2O_5 uptake coefficients on aged biomass burning particles in the UTLS are significantly lower than those used in model parameterizations

Abstract

Heterogeneous chemical cycles of pyrogenic nitrogen and halides influence tropospheric ozone and affect the stratosphere during extreme pyrocumulonimbus (PyroCB) events. We report field-derived N_2O_5 uptake coefficients, $\gamma(N_2O_5)$, and $ClNO_2$ yields, $\varphi(ClNO_2)$, from two aircraft campaigns observing fresh smoke in the lower and mid troposphere and processed/aged smoke in the upper troposphere and lower stratosphere (UTLS). Derived $\varphi(ClNO_2)$ varied across the full 0–1 range but was typically < 0.5 and smallest in a PyroCB (< 0.05). Derived $\gamma(N_2O_5)$ was low in agricultural smoke (0.2–3.6 $\times 10^{-3}$), extremely low in mid-tropospheric wildfire smoke (0.1×10^{-3}), but larger in PyroCB processed smoke ($0.7–5.0 \times 10^{-3}$). Aged BB aerosol in the UTLS had a higher median $\gamma(N_2O_5)$ of 17×10^{-3} that increased with sulfate and liquid water, but that was nevertheless 1–2 orders of magnitude lower than values for aqueous sulfuric aerosol used in stratospheric models.

Plain Language Summary

The injection of reactive material into Earth's atmosphere from fires affects atmospheric composition at regional and hemispheric scales. Reported stratospheric ozone depletion during extreme events, such as the 2020 Australian wildfires, illustrates one example of fire impacts and the role of heterogeneous (gas-particle) processes. We report field quantification of rates and product yields from airborne observations of smoke. Extremely slow heterogeneous reaction rates on young smoke increase with transport and aging, but upper atmospheric values are still a factor of 10 slower than parameterizations used in stratospheric models. Heterogeneous production of $ClNO_2$, a major lower atmospheric chlorine activation pathway, may be active on biomass burning aerosol in the upper atmosphere.

1 Introduction

Biomass burning (BB) impacts global atmospheric chemical processes and is increasing regionally due to climate-change-induced trends in fire weather [*Jones et al.*, 2022]. Fires emit nitrogen oxides ($NO + NO_2 = NO_x$), volatile organic compounds (VOCs) and aerosol that affect tropospheric oxidants [*Koss et al.*, 2018]. Roughly 10% of global inorganic chloride enters the atmosphere by BB [*Wang et al.*, 2019], and a small fraction may be subsequently activated to inorganic chlorine radicals. The co-emission of NO_x and VOCs enhances tropospheric O_3 globally on a scale comparable to, or greater than, urban pollution [*Bourgeois et al.*, 2021; *Xu et al.*, 2021].

Large wildfires can form pyrocumulonimbus (PyroCB) towers [*Peterson et al.*, 2021; *Peterson et al.*, 2022] that loft pyrogenic emissions to the upper troposphere / lower stratosphere (UTLS). Aerosol injection from the 2019–2020 Australian New Year fires altered the partitioning of total reactive chlorine (Cl_y) and nitrogen (NO_y) species and led to stratospheric O_3 loss through heterogeneous reactions [*Bernath et al.*, 2022; *Solomon et al.*, 2022; *Solomon et al.*, 2023; *Strahan et al.*, 2022]. One of the major heterogeneous reactions is uptake of N_2O_5, which in stratospheric models produces exclusively nitric acid, HNO_3 [*Küll et al.*, 2002; *Zambri et al.*, 2019].

$$N_2O_{5(g)} + H_2O_{(l)} \rightarrow 2HNO_{3(g)} \qquad (R1, \gamma)$$

Here, γ is the reactive uptake coefficient [*Ravishankara*, 1997]. Reaction (1) influences NO_x and O_3 in both the stratosphere and troposphere by altering the partitioning of reactive nitrogen and the availability of NO_x [*Dentener and Crutzen*, 1993; *Solomon*, 1999].

Tropospheric observations have shown substantial yields of nitryl chloride, $ClNO_2$, from chloride-containing aerosol [*McDuffie et al.*, 2018a], represented below as reaction with HCl.

$$N_2O_{5(g)} + HCl_{(aq)} \rightarrow ClNO_{2(g)} + HNO_{3(g)} \qquad (R2, \phi)$$

Photolysis of $ClNO_2$ produces Cl. The yield, ϕ, for R2 is the molar ratio of $ClNO_2$ produced per N_2O_5 reacted. Due in part to the lack of chloride partitioning to highly-acidic stratospheric aerosol, R2 has been considered an unimportant contribution to stratospheric halogen activation [*Solomon*, 1999] despite its prevalence in the troposphere. Figure 1 illustrates biomass burning emissions to and heterogeneous chemistry in different regions of the atmosphere.

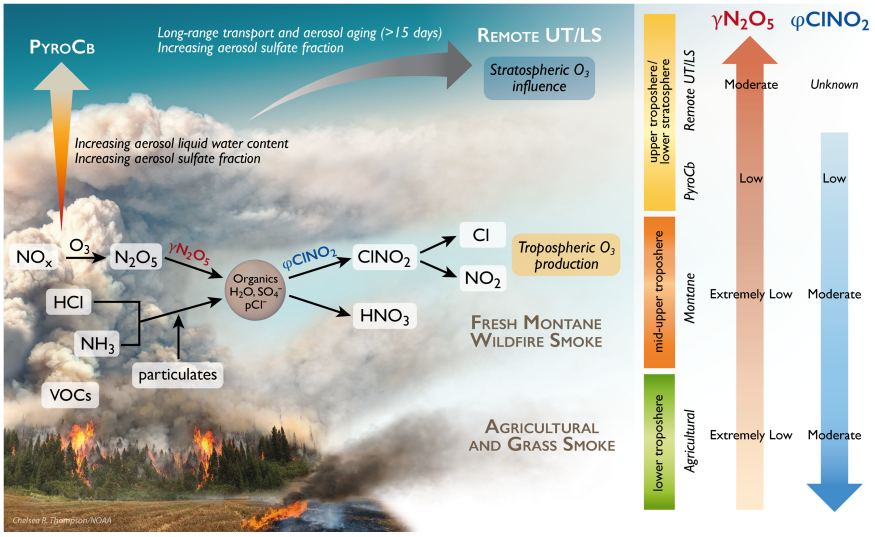

Figure 1. Biomass burning emission to different altitudes and heterogeneous chemistry of N_2O_5 and $ClNO_2$. Arrows on the right-hand side illustrate trends in heterogeneous parameters, $\gamma(N_2O_5)$ and $\phi(ClNO_2)$, determined from aircraft observations in this work**.**

Rates and yields of N_2O_5 heterogeneous chemistry on BB particles are uncertain, especially in the UTLS [*Solomon et al.*, 2022; *Strahan et al.*, 2022; *Yu et al.*, 2021]. Models assume similarity between BB and volcanic particles but are unable to reproduce remote sensing observations of Cl_y and NO_y, suggesting substantial differences in heterogeneous chemistry. There exist limited BB laboratory studies on $\gamma(N_2O_5)$ or $\phi(ClNO_2)$ [*Ahern et al.*, 2018; *Goldberger et al.*, 2019; *Jahl et al.*, 2021] and, to our knowledge, there are no field-derived values. Tropospheric and stratospheric models of BB impacts are poorly constrained for $\gamma(N_2O_5)$ and have not considered $\phi(ClNO_2)$.

We present aircraft observations of N_2O_5, $ClNO_2$ and field-derived values for $\gamma(N_2O_5)$ and $\varphi(ClNO_2)$ in smoke. The analysis utilizes aircraft observations from the 2019 Fire Influence on Regional to Global Environments and Air Quality (FIREX-AQ) campaign [*Warneke et al.*, 2023] and the 2017–2018 Atmospheric Tomography mission (ATom) [*Thompson et al.*, 2022]. We derive $\gamma(N_2O_5)$ and $\varphi(ClNO_2)$ for montane and agricultural smoke in the troposphere and a

PyroCB injection of smoke to the upper troposphere from FIREX-AQ. We derive $\gamma(N_2O_5)$ for stratospheric BB-influenced aerosol from ATom. Derived N_2O_5 uptake coefficients are considerably lower than current model parameterizations. Halogen activation through $ClNO_2$ from NO_x and particulate chloride (pCl^-) is prevalent in low altitudes and possible, yet unquantified, at high altitude.

2 Results and Discussion

2.1 $ClNO_2$ and N_2O_5 Observations

Figure 2A shows the flight track of the NASA DC-8 aircraft sampling the Williams Flats fire during FIREX-AQ on 3 Aug 2019 colored and sized by observed $ClNO_2$. Both N_2O_5 and $ClNO_2$ exhibit clear enhancements despite significant photolysis rates of NO_3 (jNO_3) (Figure 2B-C). These enhancements are associated with CO, a smoke tracer, and rapid (>1 ppbv hr^{-1}) NO_3 production, $P(NO_3) = k[NO_2][O_3]$, where k is the bimolecular rate coefficient for reaction of NO_2 with O_3.

Median j_{NO_3} at the center of wildfire and agriculture plume transects (0.14 s^{-1} and 0.19 s^{-1} respectively) were 15–30% lower than values outside of plumes (0.16 and 0.20 s^{-1} respectively). In large wildfire plumes jNO_3 attenuation was a factor of ten or more (Figure 2B and C), but small agricultural plumes exhibited no attenuation (Figure S1). Previous analyses of FIREX-AQ plumes found that NO_3 photolysis and reaction with NO are not major NO_3 loss pathways regardless of time of day [*Decker et al.*, 2021a; *Decker et al.*, 2021b]. Rapid $P(NO_3)$ together with large concentrations of highly reactive VOCs and aerosol surface area control NO_3 and N_2O_5 chemistry. Plumes with measurable daytime N_2O_5 provide measures of NO_3 reactivity and N_2O_5 heterogeneous uptake for these species that are otherwise important only at night in non-fire environments.

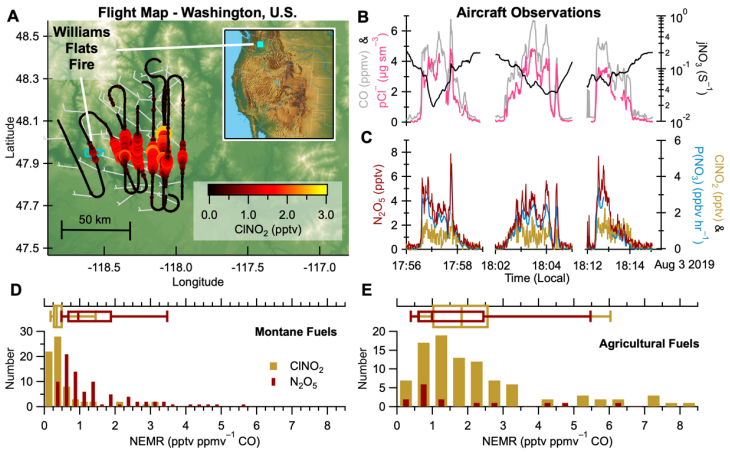

Figure 2. A. NASA DC-8 flight tracks colored and sized by $ClNO_2$ mixing ratio for the Williams Flats fire plume on Aug 3. The inset map shows the approximate location of sampling in Washington State. **B.** Observations of CO (grey), pCl^- (pink), and *jNO3* (black) and **C.** N_2O_5 (red), $ClNO_2$ (yellow) and $P(NO_3)$ (blue) for a subset of crosswind plume transects. **D & E.** Histogram of N_2O_5 and $ClNO_2$ NEMRs from all montane (D) and agricultural (E) fires. Box plots show 10th, 25th, 50th, 75th, and 90th percentiles.

The Normalized Excess Mixing Ratio (NEMR) measures the above background enhancements of a compound *x* relative to the smoke tracer CO (Table S2 and Figure S2-S4). The median N_2O_5 NEMR was 1.0 pptv ppmv^{-1} CO for both agricultural and montane fire groups (Figure 2D and E).The $ClNO_2$ NEMRs, by contrast, differ by a factor of ~6 between montane (0.3 pptv ppmv^{-1}) and agricultural (1.8 pptv ppmv^{-1}) fuels. Agricultural and grass burning emits more Cl^- per kg of fuel burned (emission factor) when compared to temperate and boreal forest burning [*Akagi et al.*, 2011; *Liu et al.*, 2016; *May et al.*, 2014]. Despite considerable variability, the greater median $ClNO_2$ NEMR for agricultural fires is consistent with the observed differences in particulate chloride (pCl^-). DC-8 and Twin Otter observations of the above background pCl^- show that agricultural and grass smoke contains roughly 16× more pCl^- by mass than montane smoke (Text S2 and Figure S5).

2.2 Montane and Agricultural Smoke

To derive $\gamma(N_2O_5)$ from agricultural smoke, we use the calculated NEMR of $ClNO_2$ as a function of the physical plume age shown in Figure 3A. We combine the calculated $ClNO_2$ NEMRs with the relationship between $\gamma(N_2O_5)$ and $\varphi(ClNO_2)$ below to estimate a $\gamma(N_2O_5)$.

$$\gamma(N_2O_5) = 4 \times \frac{k_{N_2O_5}}{c \times SA} \quad (1)$$

$$\phi(ClNO_2) = \frac{k_{ClNO_2}}{k_{N_2O_5}} \quad (2)$$

Here c is the mean molecular speed of N_2O_5 and SA is the aerosol surface area density. Data are arbitrarily separated into low and high NEMR groups. The biexponential fit represents first-order formation (k_{ClNO_2}) and photolytic loss (j_{ClNO_2}) of $ClNO_2$. Constraining the fit to an observed median photolysis rate of j_{ClNO_2} = 3.3 × 10^{-4} s^{-1} (Figure S6A) we find k_{ClNO_2} = 2.0–5.8 × 10^{-4} s^{-1}. Aerosol surface area can vary widely across a plume transect and therefore we chose a range (2–11 × 10^3 μm^2 cm^{-3}) of observed SA representative of most observations in Figure 3A (Figure S6B) and present a sensitivity analysis to this choice in Figure S6C. Finally, we use a median observed temperature of 296 K to find $\gamma(N_2O_5) \times \varphi(ClNO_2)$ = 0.3–4.7 × 10^{-3}.

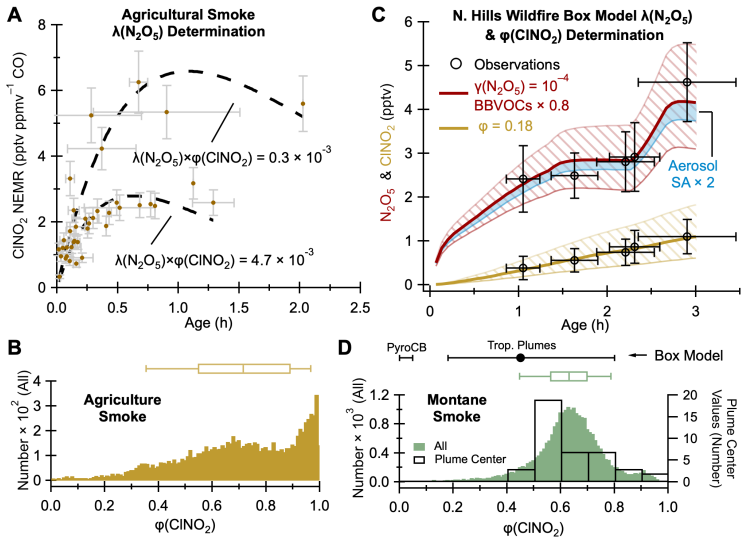

Figure 3. A. Agricultural fire $ClNO_2$ NEMRs vs. plume age. Dashed lines show biexponential fits (see text). **B.** Parametrized $\varphi(ClNO_2)$ of agricultural smoke. **C.** Box model results (lines) compared to observations (markers) of N_2O_5 and $ClNO_2$ from the July 29 North Hills smoke plume with $\gamma(N_2O_5) = 10^{-4}$. The hashed area shows changes to VOCs (N_2O_5) or yield ($ClNO_2$) that encompass observational uncertainty. Transparent blue area shows sensitivity to a factor of 2 increase in aerosol surface area. The apparent discontinuity of N_2O_5 in the model is due to a reduction in the photolysis rate at sunset (2.5 h of age). **D.** Parameterized $\varphi(ClNO_2)$ for montane smoke (filled bars) and transect center observations used in the box model (empty bars). Box model derived $\varphi(ClNO_2)$ is shown as horizontal ranges in black. The black marker indicates the average of the five modeled plumes sampled in the lower troposphere. The range on the model-derived $\varphi(ClNO_2)$ shows the range of the five modeled plumes. Note that within observation uncertainty the full range is 0-1

To estimate $\varphi(ClNO_2)$ we use a laboratory-based parameterization based on observed pCl^- and calculated liquid water content (LWC), hereafter referred to as parameterized $\phi(ClNO_2)$ (section 2.2, S1.4). Figure 3B shows parameterized $\varphi(ClNO_2)$ for all 1 Hz agriculture smoke observations, with median $\varphi(ClNO_2)$ of 0.72. When considering only observations in Figure 2A, used to determine $\gamma(N_2O_5)$, the median is 0.77. Previous field comparisons have shown that parameterized $\varphi(ClNO_2)$ is likely an upper limit [*McDuffie et al.*, 2018b], and therefore the derived $\gamma(N_2O_5)$ is a lower limit range of $0.2–3.6 \times 10^{-3}$.

Montane smoke plumes included several cross-wind transects downwind, which allows for $\gamma(N_2O_5)$ and $\varphi(ClNO_2)$ determination in individual plumes using a constrained 0-D chemical box model [*Decker et al.*, 2021a]. Model input values of $\gamma(N_2O_5)$ were varied between 10^{-4} and 10^{-1} to minimize the difference between the model and observations of N_2O_5. The modeled N_2O_5 is sensitive to NO_3 loss to reactions with VOCs. The model uses VOC emissions from laboratory burn emissions inventories, and these are also varied to improve the agreement between modeled and observed N_2O_5. A comparison of modeled and observed VOCs shows that the majority of the observation-model comparisons remain within the observation uncertainty. Lastly, $\varphi(ClNO_2)$ is varied between 0 and 1. Figures S7-S12 show complete model and observation comparisons.

Figure 3C shows a representative model to observation comparison for N_2O_5 and $ClNO_2$. In all model runs, a $\gamma(N_2O_5)$ of 10^{-4} (one order of magnitude precision, see Figure S7) best reproduces N_2O_5 observations. In these five cases, values of $\gamma(N_2O_5) \geq 10^{-3}$ cannot recreate the N_2O_5 observations without near or complete removal of VOCs, and values of $\gamma(N_2O_5) < 10^{-4}$ require $\varphi(ClNO_2) > 1$ to reproduce $ClNO_2$.

The box model derived $\varphi(ClNO_2)$ ranges from 0.18–0.80 but spans the entire 0-1 range when considering the $ClNO_2$ observational uncertainty (Figure S13). The average model-derived $\varphi(ClNO_2)$ is 0.45 (Figure 3D, black marker). The average of transect-center-parameterized $\varphi(ClNO_2)$ is 0.65, similar to the average of all parameterized $\varphi(ClNO_2)$ of 0.62. Parameterized $\varphi(ClNO_2)$ exceeds the box model, similar to previous field derivations [*McDuffie et al.*, 2018b], although >90% of parameterized $\varphi(ClNO_2)$ lies within the box model derived range (Figure 3D). Lastly, the derived $\varphi(ClNO_2)$ of agricultural smoke is generally greater than montane smoke, consistent with the greater pCl^- in the former.

Values of $\gamma(N_2O_5)$ derived here are smaller than values determined in urban air ($\gamma(N_2O_5)$ 10^{-3} - 10^{-1} [*Brown and Stutz*, 2012; *McDuffie et al.*, 2018a] and comparable to or lower than a limited number of laboratory studies. A chamber study of pyrogenic aerosol for a wire grass fuel

(2.8–6 ± 0.6 × 10^{-3}) and a long leaf pine needle fuel (2.5–3.2 ± 0.4 × 10^{-3}) [*Goldberger et al.*, 2019] are similar to our agricultural fuels result. A flow-tube study of pyrogenic aerosol identified an increase of $\gamma(N_2O_5)$ for high-chloride-containing BB fuels at relative humidity (RH) >80% [*Jahl et al.*, 2021]. This is similar to the average RH (70%) for the agricultural smoke plumes here (Figure S14) and consistent with the observation of greater pCl^- (Figure S5) and larger $\gamma(N_2O_5)$ values (Figure 3) compared to montane smoke.

2.3 PyroCB Processed Smoke

The DC-8 sampled a PyroCB event from the Williams Flats fire on August 8 that reached 6–10 km above sea level, or 5.6 to 1.6 km below the mean tropopause height. We separate our analysis by plume number and transect number as defined by [*Peterson et al.*, 2022].

Observed $P(NO_3)$ and N_2O_5 (Figure 4A) demonstrate the potential for heterogeneous chemistry in the PyroCB injection to the upper atmosphere. Calculated N_2O_5 NEMR increases with calculated physical plume age when separated by plume number (Figure 4B). Enhancement of pCl^- (Figure 4C) demonstrates the potential for $ClNO_2$ production. However, observations of $ClNO_2$ remained at or below the 1Hz I^- CIMS detection limit of 0.05 pptv in Figure 4A and D, limiting the ability to quantify its production. Figure S15 shows that the $ClNO_2$ signal within all PyroCB smoke observations (average ± 1-σ of 0.03 ± 0.10 pptv) is statistically significantly greater ($p<0.001$) than signal outside of the plume (average ± 1-σ of 0.02 ± 0.06 pptv), but the data do not allow quantification of the amount of $ClNO_2$ within the PyroCB.

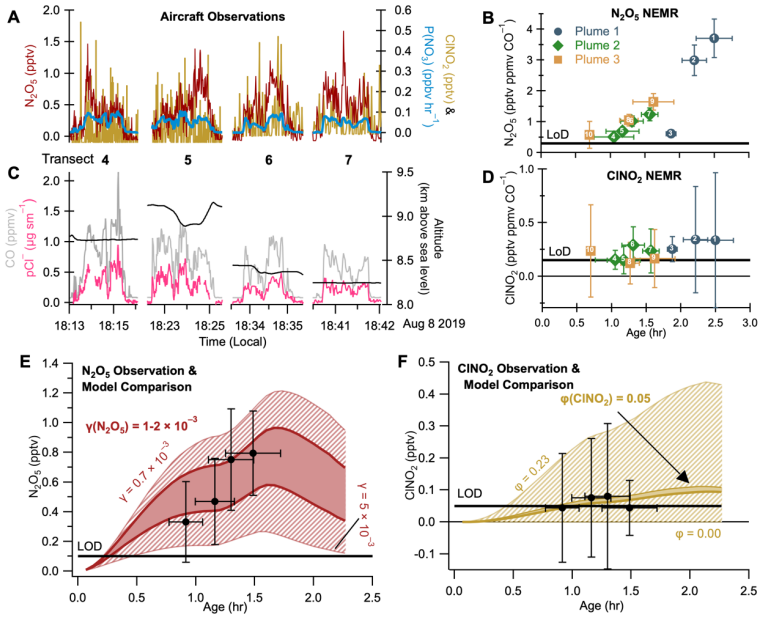

Figure 4. NASA DC-8 observations in a PyroCB. Panels A and B show plume 2 observations only (transects 4–7). **A & C.** Observations of N_2O_5 (red), $ClNO_2$ (yellow) and $P(NO_3)$ (blue), CO (grey), pCl^- (pink), and jNO_3 (black). **B &D.** NEMRs of N_2O_5 and $ClNO_2$. Markers and colors indicate the plume number, and white numbers indicate the transect number. The thick black line indicates the limit of detection (LoD). **E.** Transect center observations of N_2O_5 (black) for plume 2 compared to the model N_2O_5 for a range (7×10^{-4}–5×10^{-3}) of $\gamma(N_2O_5)$. **F.** Transect center observations of $ClNO_2$ (black) for plume 2 compared to the model-derived $ClNO_2$. Solid color is

the result of a $\varphi(ClNO_2) = 0.05$ and a $\gamma(N_2O_5) = 1–2 \times 10^{-3}$ and the hashed area shows a range of possible $\varphi(ClNO_2)$.

Aerosol data are unavailable for plume 3, and plume 1 did not have sufficient semi-Lagrangian crosswind transects required to constrain the model. Therefore, the box model is used to derive $\gamma(N_2O_5)$ and to place an upper limit on $\varphi(ClNO_2)$ for plume 2 only. The model derived $\gamma(N_2O_5) = 0.7–5.0 \times 10^{-3}$ (Figure 4E), which is a factor of 7 – 50 × greater than the $\gamma(N_2O_5)$ values from plumes produced by the same fire but sampled in the lower troposphere.

The model predicts $\varphi(ClNO_2) < 0.05$ to match observations at or below the detection limit (or 0.05 at the LoD), although $\varphi(ClNO_2)$ may be up to 0.23 within the 1-σ determined $ClNO_2$ measurement uncertainty (15% + 0.05 pptv). The average parameterized $\varphi(ClNO_2)$ (0.53) is also lower than tropospheric smoke from the same fire (Figure S16) as a result of increased calculated liquid water fraction (LWF, Figure S17) in the PyroCB. The presence of sufficient pCl^- for average parameterized $\phi(ClNO_2) > 0.5$ suggests that $ClNO_2$ production may occur in PyroCB transported smoke, even if it was observed only at the detection limit in this daytime flight.

2.4 Aged UTLS pyrogenic aerosol

Observations from the ATom campaign provide N_2O_5 observations in the UTLS. We separate our analysis into background and pyrogenic-influenced (defined as >75% of aerosol number concentration containing pyrogenic markers, see SI). The pyrogenic aerosol is estimated to have a physical age of >15 days. A diel model built on the framework of previous model determinations of $\gamma(N_2O_5)$ in the lower troposphere [*McDuffie et al.*, 2018a] is constrained to chemical observations (see SI).

The diel model predicts the median $\gamma(N_2O_5)$ from all background UTLS samples (N=3483) is 2.9×10^{-2} as shown in Figure 5A (grey box and whiskers). The pyrogenic-influenced aerosol has a median $\gamma(N_2O_5)$ of 1.7×10^{-2} (Figure 4A, brown) which is significantly different ($p < 0.001$) than the background aerosol. We also consider a smaller subset of pyrogenic influenced aerosol from ATom previously identified by [*Katich et al.*, 2023] to have originated from PyroCB influence. The resulting $\gamma(N_2O_5)$ of 2.5×10^{-2} is significantly ($p = 0.01$) less than background UTLS aerosol, and greater than our selection of pyrogenic influenced aerosol (Figure S18). Overall, the model predicts that pyrogenic aerosol has a lower rate of N_2O_5 uptake than background UTLS aerosol, yet substantially greater than pyrogenic aerosol in young tropospheric plumes.

The differences in $\gamma(N_2O_5)$ across agricultural, montane, PyroCb, and UTLS data are associated with increased aerosol sulfate fraction. Figure 5B shows a positive trend in $\log(\gamma(N_2O_5))$ as a function of aerosol sulfate fraction distribution. The median sulfate fraction was 1, 5, 9 and 42% in recently-emitted montane, PyroCB, agricultural and aged stratospheric BB aerosol, respectively. Laboratory studies suggest organic coatings inhibit N_2O_5 uptake, which is generally dependent on the organic layer composition and relative humidity [*Gaston et al.*, 2014]. Conversely, increasing sulfate fraction is associated with increasing $\gamma(N_2O_5)$ [*McDuffie et al.*, 2018a]. Sulfate in tropospheric BB plumes arises from oxidation of pyrogenic SO_2 [*Rickly et al.*, 2022], whereas pyrogenic-influenced aerosol in the UTLS takes up sulfate during aging.

Current stratospheric models of BB impacts on stratospheric processes [*Strahan et al.*, 2022; *Yu et al.*, 2021] use a $\gamma(N_2O_5)$ based on aqueous sulfate aerosol. Figure 5C shows $\gamma(N_2O_5)$

values from BB influenced aerosol are a factor of 10–100 lower than pure aqueous sulfate particles [*Burkholder et al.*, 2020]. BB particles are expected to condense organics from low-volatility VOC oxidation products [*Palm et al.*, 2020], forming organic layers that may reduce $\gamma(N_2O_5)$. Evidence of organic markers on stratospheric aerosol was found in some studies of stratospheric BB aerosol [*Bernath et al.*, 2022; *Katich et al.*, 2023], and BB aerosol markers are used here, by definition, to separate BB aerosol from background aerosol.

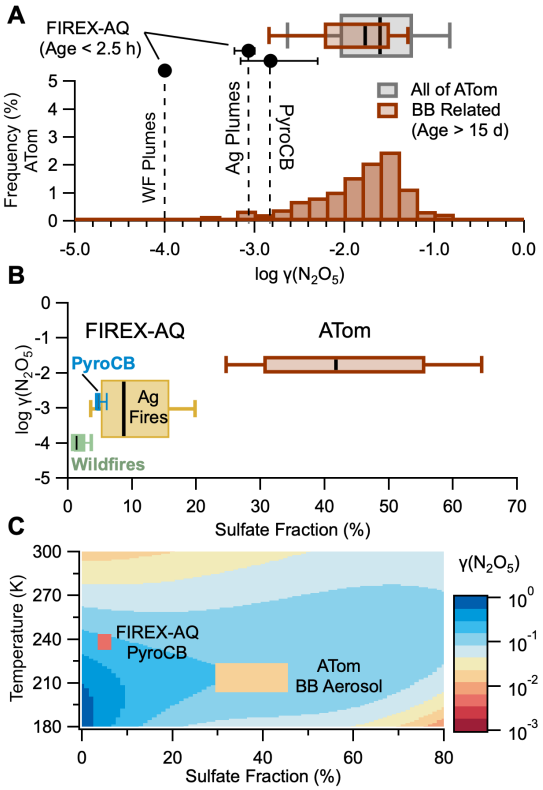

Figure 5. A. Comparison of the model-derived $\gamma(N_2O_5)$ from FIREX-AQ and ATom. Markers show FIREX-AQ results, and the histograms show ATom BB-related $\gamma(N_2O_5)$. The box and whisker plots show the ATom BB-related (brown) and all of the ATom (grey) results from the UTLS. **B**. Log $\gamma(N_2O_5)$ vs aerosol sulfate fraction for FIREX-AQ and ATom. **C**. $\gamma(N_2O_5)$ parametrization from [*Burkholder et al.*, 2020] for aqueous sulfate particles used in stratospheric models compared to results from this work. Marker size represents the interquartile range of temperature and sulfate fraction in this work.

These results indicate $\gamma(N_2O_5)$ values increase for BB particles transported from the troposphere into the UTLS, but never reach values used in stratospheric models. Injection of the chloride-containing aerosol observed in montane smoke or repartitioning of gas phase HCl to particulate organics or reduced nitrogen [*Solomon et al.*, 2023] may result in a non-zero $ClNO_2$ yield, thus introducing chlorine activation pathways currently not considered. Observations presented here cannot quantify $ClNO_2$ production on BB particles transported through a PyroCB but demonstrate potential for this process. Observations of diffuse BB influenced particles in the UTLS from ATom do not have reliable $ClNO_2$ measurements, such that we are unable to assess $ClNO_2$ production on aged, dilute UTLS BB influenced particles. Concentrated BB plumes transported to the stratosphere through PyroCB events, such as the 2020 Australian fires, should

have heterogeneous chemistry similar to that observed here. Recent analysis of high-altitude aircraft data suggests a ubiquitous influence of such events on stratospheric aerosol composition [*Katich et al.*, 2023].

3 Conclusions

Uptake coefficients for N_2O_5 determined from in situ observations are lower on BB aerosol than current model parameterizations. Figure 1 illustrates the observed trends in uptake coefficients from the lower to the upper atmosphere. The $\gamma(N_2O_5)$ on dilute smoke-impacted particles derived in this study is already lower than model parameterizations but likely represents an upper limit for more concentrated smoke such as the 2020 Australian wildfires. We therefore suggest that models of the smoke impact to the UTLS will require revised parameterizations with reduced uptake coefficients.

Second [*Solomon et al.*, 2023] show that chloride uptake by the organic phase of smoke aerosol increases heterogeneous reaction rates of halogen-containing species, thereby activating chlorine radicals that participate in ozone destruction cycles. Our results demonstrate that N_2O_5 uptake on chloride-containing smoke particles produces $ClNO_2$ in the lower atmosphere and has the potential to do so in the upper atmosphere, particularly with increased chloride partitioning to the aerosol phase. We suggest that $ClNO_2$ formation from N_2O_5 uptake on smoke particles injected into the stratosphere during large PyroCB events may be a component of smoke-induced halogen activation cycles that influence stratospheric ozone.

Acknowledgments

We thank Charles A. Brock for particle sizing data from ATom. We thank William H. Brune and Alexander B. Thames for OH/HO_2 data from ATom. We thank Daniel M. Murphy for PALMS particle type data from ATom. ZCJD, GAN, KA, IB, PCJ, MMC, DAD, AF, JLJ, DP, JP, PR, MAR, CRT, CW, and CCW, were supported by the NOAA cooperative agreement NA17OAR4320101. PCJ, HG, BAN, DP, DAD, and JLJ acknowledge support from NASA Earth Sciences Division (grant nos. NNX15AH33A, 80NSSC18K0630 and 80NSSC21K1451). C.D.F., B.B.P., and J.A.T. acknowledge support from the NOAA OAR Climate Program Office (grant no. NA17OAR4310012) CDF acknowledges support from the Future Investigators in NASA Earth and Space Science and Technology (FINESST) Grant Number 80NSSC20K1612. SRH and KU acknowledge support from NASA Earth Sciences Division (grant nos. 80NSSC18K0638 and NNX15AG71A). Participation in ATom Mission flights by G.P.S., K.D.F., and D.M.M. was supported by NOAA climate funding (no. NNH15AB12I).

Data Availability Statement

The aircraft data used in the study are publicly available at https://www-air.larc.nasa.gov/missions/firex-aq/.

References

Ahern, A. T., L. Goldberger, L. Jahl, J. Thornton, and R. C. Sullivan (2018), Production of N_2O_5 and $ClNO_2$ through Nocturnal Processing of Biomass-Burning Aerosol, *Environmental Science & Technology*, *52*(2), 550-559, 10.1021/acs.est.7b04386.

Akagi, S. K., R. J. Yokelson, C. Wiedinmyer, M. J. Alvarado, J. S. Reid, T. Karl, J. D. Crounse, and P. O. Wennberg (2011), Emission factors for open and domestic biomass burning for use in atmospheric models, *Atmos. Chem. Phys.*, *11*(9), 4039-4072, 10.5194/acp-11-4039-2011.

Bernath, P., C. Boone, and J. Crouse (2022), Wildfire smoke destroys stratospheric ozone, *Science*, *375*(6586), 1292-1295, 10.1126/science.abm5611.

Bourgeois, I., J. Peischl, J. A. Neuman, S. S. Brown, C. R. Thompson, K. C. Aikin, H. M. Allen, H. Angot, E. C. Apel, C. B. Baublitz, J. F. Brewer, P. Campuzano-Jost, R. Commane, J. D. Crounse, B. C. Daube, J. P. DiGangi, G. S. Diskin, L. K. Emmons, A. M. Fiore, G. I. Gkatzelis, A. Hills, R. S. Hornbrook, L. G. Huey, J. L. Jimenez, M. Kim, F. Lacey, K. McKain, L. T. Murray, B. A. Nault, D. D. Parrish, E. Ray, C. Sweeney, D. Tanner, S. C. Wofsy, and T. B. Ryerson (2021), Large contribution of biomass burning emissions to ozone throughout the global remote troposphere, *Proceedings of the National Academy of Sciences*, *118*(52), e2109628118, 10.1073/pnas.2109628118.

Brown, S. S., and J. Stutz (2012), Nighttime Radical Observations and Chemistry, *Chem. Soc. Reviews*, *41*, 6405-6447, DOI: 10.1039/c2cs35181a.

Burkholder, J. B., J. P. D. Abbatt, C. Cappa, T. S. Dibble, C. E. Kolb, V. L. Orkin, D. M. Wilmouth, S. P. Sander, J. R. Barker, J. D. Crounse, R. E. Huie, M. J. Kurylo, C. J. Percival, and P. H. Wine (2020), *Chemical Kinetics and Photochemical Data for Use in Atmospheric Studies*, JPL Publication 19-5, Pasadena, CA.

Decker, Z. C. J., M. A. Robinson, K. C. Barsanti, I. Bourgeois, M. M. Coggon, J. P. DiGangi, G. S. Diskin, F. M. Flocke, A. Franchin, C. D. Fredrickson, G. I. Gkatzelis, S. R. Hall, H. Halliday, C. D. Holmes, L. G. Huey, Y. R. Lee, J. Lindaas, A. M. Middlebrook, D. D. Montzka, R. Moore, J. A. Neuman, J. B. Nowak, B. B. Palm, J. Peischl, F. Piel, P. S. Rickly, A. W. Rollins, T. B. Ryerson, R. H. Schwantes, K. Sekimoto, L. Thornhill, J. A. Thornton, G. S. Tyndall, K. Ullmann, P. Van Rooy, P. R. Veres, C. Warneke, R. A. Washenfelder, A. J. Weinheimer, E. Wiggins, E. Winstead, A. Wisthaler, C. Womack, and S. S. Brown (2021a), Nighttime and daytime dark oxidation chemistry in wildfire plumes: an observation and model analysis of FIREX-AQ aircraft data, *Atmos. Chem. Phys.*, *21*(21), 16293-16317, 10.5194/acp-21-16293-2021.

Decker, Z. C. J., S. Wang, I. Bourgeois, P. Campuzano Jost, M. M. Coggon, J. P. DiGangi, G. S. Diskin, F. M. Flocke, A. Franchin, C. D. Fredrickson, G. I. Gkatzelis, S. R. Hall, H. Halliday, K. Hayden, C. D. Holmes, L. G. Huey, J. L. Jimenez, Y. R. Lee, J. Lindaas, A. M. Middlebrook, D. D. Montzka, J. A. Neuman, J. B. Nowak, D. Pagonis, B. B. Palm, J. Peischl, F. Piel, P. S. Rickly, M. A. Robinson, A. W. Rollins, T. B. Ryerson, K. Sekimoto, J. A. Thornton, G. S. Tyndall, K. Ullmann, P. R. Veres, C. Warneke, R. A. Washenfelder, A. J. Weinheimer, A. Wisthaler, C. Womack, and S. S. Brown (2021b), Novel Analysis to Quantify Plume Crosswind Heterogeneity Applied to Biomass Burning Smoke, *Environmental Science & Technology*, *55*(23), 15646-15657, 10.1021/acs.est.1c03803.

Dentener, F. J., and P. J. Crutzen (1993), Reaction of N_2O_5 on Tropospheric Aerosols: Impact on the Global Distributions of NO_x, O_3, and OH, *J. Geophys. Res.*, *98*(D4), 7149-7163.

Gaston, C. J., J. A. Thornton, and N. L. Ng (2014), Reactive uptake of N_2O_5 to internally mixed inorganic and organic particles: the role of organic carbon oxidation state and inferred organic phase separations, *Atmos. Chem. Phys.*, *14*(11), 5693-5707, 10.5194/acp-14-5693-2014.

Goldberger, L. A., L. G. Jahl, J. A. Thornton, and R. C. Sullivan (2019), N_2O_5 reactive uptake kinetics and chlorine activation on authentic biomass-burning aerosol, *Environmental Science: Processes & Impacts*, *21*(10), 1684-1698, 10.1039/C9EM00330D.

Jahl, L. G., B. B. Bowers, L. G. Jahn, J. A. Thornton, and R. C. Sullivan (2021), Response of the Reaction Probability of N2O5 with Authentic Biomass-Burning Aerosol to High Relative Humidity, *ACS Earth and Space Chemistry*, *5*(10), 2587-2598, 10.1021/acsearthspacechem.1c00227.

Jones, M. W., J. T. Abatzoglou, S. Veraverbeke, N. Andela, G. Lasslop, M. Forkel, A. J. P. Smith, C. Burton, R. A. Betts, G. R. van der Werf, S. Sitch, J. G. Canadell, C. Santín, C. Kolden, S. H. Doerr, and C. Le Quéré (2022), Global and Regional Trends and Drivers of Fire Under Climate Change, *Reviews of Geophysics*, *60*(3), e2020RG000726, https://doi.org/10.1029/2020RG000726.

Katich, J. M., E. C. Apel, I. Bourgeois, C. A. Brock, T. P. Bui, P. Campuzano-Jost, R. Commane, B. Daube, M. Dollner, M. Fromm, K. D. Froyd, A. J. Hills, R. S. Hornbrook, J. L. Jimenez, A. Kupc, K. D. Lamb, K. McKain, F. Moore, D. M. Murphy, B. A. Nault, J. Peischl, A. E. Perring, D. A. Peterson, E. A. Ray, K. H. Rosenlof, T. Ryerson, G. P. Schill, J. C. Schroder, B. Weinzierl, C. Thompson, C. J. Williamson, S. C. Wofsy, P. Yu, and J. P. Schwarz (2023), Pyrocumulonimbus affect average stratospheric aerosol composition, *Science*, *379*(6634), 815-820, 10.1126/science.add3101.

Koss, A. R., K. Sekimoto, J. B. Gilman, V. Selimovic, M. M. Coggon, K. J. Zarzana, B. Yuan, B. M. Lerner, S. S. Brown, J. L. Jimenez, J. Krechmer, J. M. Roberts, C. Warneke, R. J. Yokelson, and J. de Gouw (2018), Non-methane organic gas emissions from biomass burning: identification, quantification, and emission factors from PTR-ToF during the FIREX 2016 laboratory experiment, *Atmos. Chem. Phys.*, *18*(5), 3299-3319, 10.5194/acp-18-3299-2018.

Küll, V., M. Riese, X. Tie, T. Wiemert, G. Eidmann, D. Offermann, and G. P. Brasseur (2002), NOy partitioning and aerosol influences in the stratosphere, *J. Geophys. Res.*, *107*(D23), 8183, 10.1029/2001jd001246.

Liu, X., Y. Zhang, L. G. Huey, R. J. Yokelson, Y. Wang, J. L. Jimenez, P. Campuzano-Jost, A. J. Beyersdorf, D. R. Blake, Y. Choi, J. M. St. Clair, J. D. Crounse, D. A. Day, G. S. Diskin, A. Fried, S. R. Hall, T. F. Hanisco, L. E. King, S. Meinardi, T. Mikoviny, B. B. Palm, J. Peischl, A. E. Perring, I. B. Pollack, T. B. Ryerson, G. Sachse, J. P. Schwarz, I. J. Simpson, D. J. Tanner, K. L. Thornhill, K. Ullmann, R. J. Weber, P. O. Wennberg, A. Wisthaler, G. M. Wolfe, and L. D. Ziemba (2016), Agricultural fires in the southeastern U.S. during SEAC4RS: Emissions of trace gases and particles and evolution of ozone, reactive nitrogen, and organic aerosol, *Journal of Geophysical Research: Atmospheres*, *121*(12), 7383-7414, 10.1002/2016JD025040.

May, A. A., G. R. McMeeking, T. Lee, J. W. Taylor, J. S. Craven, I. Burling, A. P. Sullivan, S. Akagi, J. L. Collett Jr, M. Flynn, H. Coe, S. P. Urbanski, J. H. Seinfeld, R. J. Yokelson, and S. M. Kreidenweis (2014), Aerosol emissions from prescribed fires in the United

States: A synthesis of laboratory and aircraft measurements, *Journal of Geophysical Research: Atmospheres*, *119*(20), 11,826-811,849, https://doi.org/10.1002/2014JD021848.

McDuffie, E., E., L. Fibiger Dorothy, P. Dubé William, F. Lopez-Hilfiker, H. Lee Ben, A. Thornton Joel, V. Shah, L. Jaeglé, H. Guo, J. Weber Rodney, J. Michael Reeves, J. Weinheimer Andrew, C. Schroder Jason, P. Campuzano-Jost, L. Jimenez Jose, E. Dibb Jack, P. Veres, C. Ebben, L. Sparks Tamara, J. Wooldridge Paul, C. Cohen Ronald, S. Hornbrook Rebecca, C. Apel Eric, T. Campos, R. Hall Samuel, K. Ullmann, and S. S. Brown (2018a), Heterogeneous N2O5 Uptake During Winter: Aircraft Measurements During the 2015 WINTER Campaign and Critical Evaluation of Current Parameterizations, *Journal of Geophysical Research: Atmospheres*, *123*(8), 4345-4372, 10.1002/2018JD028336.

McDuffie, E. E., D. L. Fibiger, W. P. Dubé, F. Lopez Hilfiker, B. H. Lee, L. Jaeglé, H. Guo, R. J. Weber, J. M. Reeves, A. J. Weinheimer, J. C. Schroder, P. Campuzano-Jost, J. L. Jimenez, J. E. Dibb, P. Veres, C. Ebben, T. L. Sparks, P. J. Wooldridge, R. C. Cohen, T. Campos, S. R. Hall, K. Ullmann, J. M. Roberts, J. A. Thornton, and S. S. Brown (2018b), $ClNO_2$ Yields From Aircraft Measurements During the 2015 WINTER Campaign and Critical Evaluation of the Current Parameterization, *Journal of Geophysical Research: Atmospheres*, *123*(22), 12,994-913,015, 10.1029/2018JD029358.

Palm, B. B., Q. Peng, C. D. Fredrickson, B. H. Lee, L. A. Garofalo, M. A. Pothier, S. M. Kreidenweis, D. K. Farmer, R. P. Pokhrel, Y. Shen, S. M. Murphy, W. Permar, L. Hu, T. L. Campos, S. R. Hall, K. Ullmann, X. Zhang, F. Flocke, E. V. Fischer, and J. A. Thornton (2020), Quantification of organic aerosol and brown carbon evolution in fresh wildfire plumes, *Proceedings of the National Academy of Sciences*, *117*(47), 29469, 10.1073/pnas.2012218117.

Peterson, D. A., M. D. Fromm, R. H. D. McRae, J. R. Campbell, E. J. Hyer, G. Taha, C. P. Camacho, G. P. Kablick, C. C. Schmidt, and M. T. DeLand (2021), Australia's Black Summer pyrocumulonimbus super outbreak reveals potential for increasingly extreme stratospheric smoke events, *npj Climate and Atmospheric Science*, *4*(1), 38, 10.1038/s41612-021-00192-9.

Peterson, D. A., L. H. Thapa, P. E. Saide, A. J. Soja, E. M. Gargulinski, E. J. Hyer, B. Weinzierl, M. Dollner, M. Schöberl, P. P. Papin, S. Kondragunta, C. P. Camacho, C. Ichoku, R. H. Moore, J. W. Hair, J. H. Crawford, P. E. Dennison, O. V. Kalashnikova, C. E. Bennese, T. P. Bui, J. P. DiGangi, G. S. Diskin, M. A. Fenn, H. S. Halliday, J. Jimenez, J. B. Nowak, C. Robinson, K. Sanchez, T. J. Shingler, L. Thornhill, E. B. Wiggins, E. Winstead, and C. Xu (2022), Measurements from inside a Thunderstorm Driven by Wildfire: The 2019 FIREX-AQ Field Experiment, *Bulletin of the American Meteorological Society*, 10.1175/BAMS-D-21-0049.1.

Ravishankara, A. R. (1997), Heterogeneous and multiphase chemistry in the troposphere, *Science*, *276*, 1058-1065.

Rickly, P. S., H. Guo, P. Campuzano-Jost, J. L. Jimenez, G. M. Wolfe, R. Bennett, I. Bourgeois, J. D. Crounse, J. E. Dibb, J. P. DiGangi, G. S. Diskin, M. Dollner, E. M. Gargulinski, S. R. Hall, H. S. Halliday, T. F. Hanisco, R. A. Hannun, J. Liao, R. Moore, B. A. Nault, J. B. Nowak, J. Peischl, C. E. Robinson, T. Ryerson, K. J. Sanchez, M. Schöberl, A. J. Soja, J. M. St. Clair, K. L. Thornhill, K. Ullmann, P. O. Wennberg, B. Weinzierl, E. B. Wiggins, E. L. Winstead, and A. W. Rollins (2022), Emission factors and evolution of

SO2 measured from biomass burning in wildfires and agricultural fires, *Atmos. Chem. Phys.*, *22*(23), 15603-15620, 10.5194/acp-22-15603-2022.

Solomon, S. (1999), Stratospheric ozone depletion: A review of concepts and history, *Reviews of Geophysics*, *37*(3), 275-316, 10.1029/1999rg900008.

Solomon, S., K. Dube, K. Stone, P. Yu, D. Kinnison, B. Toon Owen, E. Strahan Susan, H. Rosenlof Karen, R. Portmann, S. Davis, W. Randel, P. Bernath, C. Boone, G. Bardeen Charles, A. Bourassa, D. Zawada, and D. Degenstein (2022), On the stratospheric chemistry of midlatitude wildfire smoke, *Proceedings of the National Academy of Sciences*, *119*(10), e2117325119, 10.1073/pnas.2117325119.

Solomon, S., K. Stone, P. Yu, D. M. Murphy, D. Kinnison, A. R. Ravishankara, and P. Wang (2023), Chlorine activation and enhanced ozone depletion induced by wildfire aerosol, *Nature*, *615*(7951), 259-264, 10.1038/s41586-022-05683-0.

Strahan, S. E., D. Smale, S. Solomon, G. Taha, M. R. Damon, S. D. Steenrod, N. Jones, B. Liley, R. Querel, and J. Robinson (2022), Unexpected Repartitioning of Stratospheric Inorganic Chlorine After the 2020 Australian Wildfires, *Geophysical Research Letters*, *49*(14), e2022GL098290, https://doi.org/10.1029/2022GL098290.

Thompson, C. R., S. C. Wofsy, M. J. Prather, P. A. Newman, T. F. Hanisco, T. B. Ryerson, D. W. Fahey, E. C. Apel, C. A. Brock, W. H. Brune, K. Froyd, J. M. Katich, J. M. Nicely, J. Peischl, E. Ray, P. R. Veres, S. Wang, H. M. Allen, E. Asher, H. Bian, D. Blake, I. Bourgeois, J. Budney, T. P. Bui, A. Butler, P. Campuzano-Jost, C. Chang, M. Chin, R. Commane, G. Correa, J. D. Crounse, B. Daube, J. E. Dibb, J. P. DiGangi, G. S. Diskin, M. Dollner, J. W. Elkins, A. M. Fiore, C. M. Flynn, H. Guo, S. R. Hall, R. A. Hannun, A. Hills, E. J. Hintsa, A. Hodzic, R. S. Hornbrook, L. G. Huey, J. L. Jimenez, R. F. Keeling, M. J. Kim, A. Kupc, F. Lacey, L. R. Lait, J.-F. Lamarque, J. Liu, K. McKain, S. Meinardi, D. O. Miller, S. A. Montzka, F. L. Moore, E. J. Morgan, D. M. Murphy, L. T. Murray, B. A. Nault, J. A. Neuman, L. Nguyen, Y. Gonzalez, A. Rollins, K. Rosenlof, M. Sargent, G. Schill, J. P. Schwarz, J. M. S. Clair, S. D. Steenrod, B. B. Stephens, S. E. Strahan, S. A. Strode, C. Sweeney, A. B. Thames, K. Ullmann, N. Wagner, R. Weber, B. Weinzierl, P. O. Wennberg, C. J. Williamson, G. M. Wolfe, and L. Zeng (2022), The NASA Atmospheric Tomography (ATom) Mission: Imaging the Chemistry of the Global Atmosphere, *Bulletin of the American Meteorological Society*, *103*(3), E761-E790, 10.1175/BAMS-D-20-0315.1.

Wang, X., D. J. Jacob, S. D. Eastham, M. P. Sulprizio, L. Zhu, Q. Chen, B. Alexander, T. Sherwen, M. J. Evans, B. H. Lee, J. D. Haskins, F. D. Lopez-Hilfiker, J. A. Thornton, G. L. Huey, and H. Liao (2019), The role of chlorine in global tropospheric chemistry, *Atmos. Chem. Phys.*, *19*(6), 3981-4003, 10.5194/acp-19-3981-2019.

Warneke, C., J. P. Schwarz, J. Dibb, O. Kalashnikova, G. Frost, J. Al-Saad, S. S. Brown, W. A. Brewer, A. Soja, F. C. Seidel, R. A. Washenfelder, E. B. Wiggins, R. H. Moore, B. E. Anderson, C. Jordan, T. I. Yacovitch, S. C. Herndon, S. Liu, T. Kuwayama, D. Jaffe, N. Johnston, V. Selimovic, R. Yokelson, D. M. Giles, B. N. Holben, P. Goloub, I. Popovici, M. Trainer, A. Kumar, R. B. Pierce, D. Fahey, J. Roberts, E. M. Gargulinski, D. A. Peterson, X. Ye, L. H. Thapa, P. E. Saide, C. H. Fite, C. D. Holmes, S. Wang, M. M. Coggon, Z. C. J. Decker, C. E. Stockwell, L. Xu, G. Gkatzelis, K. Aikin, B. Lefer, J. Kaspari, D. Griffin, L. Zeng, R. Weber, M. Hastings, J. Chai, G. M. Wolfe, T. F. Hanisco, J. Liao, P. Campuzano Jost, H. Guo, J. L. Jimenez, J. Crawford, and F.-A. Q. S. T. The (2023), Fire Influence on Regional to Global Environments and Air Quality

(FIREX-AQ), *Journal of Geophysical Research: Atmospheres*, *128*(2), e2022JD037758, https://doi.org/10.1029/2022JD037758.

Xu, L., D. Crounse John, T. Vasquez Krystal, H. Allen, O. Wennberg Paul, I. Bourgeois, S. Brown Steven, P. Campuzano-Jost, M. Coggon Matthew, H. Crawford James, P. DiGangi Joshua, S. Diskin Glenn, A. Fried, M. Gargulinski Emily, B. Gilman Jessica, I. Gkatzelis Georgios, H. Guo, W. Hair Johnathan, R. Hall Samuel, A. Halliday Hannah, F. Hanisco Thomas, A. Hannun Reem, D. Holmes Christopher, L. G. Huey, L. Jimenez Jose, A. Lamplugh, R. Lee Young, J. Liao, J. Lindaas, J. A. Neuman, B. Nowak John, J. Peischl, A. Peterson David, F. Piel, D. Richter, S. Rickly Pamela, A. Robinson Michael, W. Rollins Andrew, B. Ryerson Thomas, K. Sekimoto, V. Selimovic, T. Shingler, J. Soja Amber, M. St. Clair Jason, J. Tanner David, K. Ullmann, R. Veres Patrick, J. Walega, C. Warneke, A. Washenfelder Rebecca, P. Weibring, A. Wisthaler, M. Wolfe Glenn, C. Womack Caroline, and J. Yokelson Robert (2021), Ozone chemistry in western U.S. wildfire plumes, *Science Advances*, *7*(50), eabl3648, 10.1126/sciadv.abl3648.

Yu, P., S. M. Davis, O. B. Toon, R. W. Portmann, C. G. Bardeen, J. E. Barnes, H. Telg, C. Maloney, and K. H. Rosenlof (2021), Persistent Stratospheric Warming Due to 2019–2020 Australian Wildfire Smoke, *Geophysical Research Letters*, *48*(7), e2021GL092609, https://doi.org/10.1029/2021GL092609.

Zambri, B., S. Solomon, D. E. Kinnison, M. J. Mills, A. Schmidt, R. R. Neely Iii, A. E. Bourassa, D. A. Degenstein, and C. Z. Roth (2019), Modeled and Observed Volcanic Aerosol Control on Stratospheric NOy and Cly, *Journal of Geophysical Research: Atmospheres*, *124*(17-18), 10283-10303, 10.1029/2019JD031111.